Quantum-classical correspondence and the transition to chaos in coupled quartic oscillators

K. M. Atkins and G. S. Ezra

Baker Laboratory, Department of Chemistry, Cornell University, Ithaca, New York 14853

In this paper we investigate the semiclassical mechanics of a system of two quartic oscillators coupled by a quartic perturbation $\gamma q_1^2 q_2^2$. Our focus is on the evolution of the quantum density of states from the integrable limit ($\gamma = 0$) to the strongly coupled regime ($\gamma = 15.0$). In the integrable limit, the Berry-Tabor analysis of the semiclassical density of states in terms of rational tori is appropriate. We extend this analysis to treat the contributions of resonant tori at the boundaries of physical action space. Computation of the power spectrum of the quantum density of states for a sequence of γ values reveals the evolution of the underlying classical periodic orbit structure. The influence of several resonant, symmetric isochronous, and tangent bifurcations on the density of states is identified. Localization of eigenstates in the vicinity of the shortest periodic orbits is also discussed.

I. INTRODUCTION

There has been much recent interest in the classical-quantum correspondence for nonintegrable systems [1,2]. Semiclassical periodic orbit theory is an essential tool in such studies [1]. Periodic orbit theory expresses the quantum mechanical density of states or matrix elements of (sufficiently smooth) operators in terms of the properties of classical periodic orbits [1,3]. These methods have been applied in atomic [4,5] and molecular [6,7] physics.

Two degree of freedom systems with homogeneous quartic potentials have been widely studied [8–17]. Early classical investigations of the $x^2 y^2$ potential suggested that the system was completely (harshly) chaotic [8]; subsequent studies have shown the existence of small stable regions in phase space [13,14]. Wave function localization or "scarring" in configuration space [10] and in phase space [12] has been examined and approximate adiabatic quantization schemes proposed for eigenvalues [10,16]. A detailed study of coupled quartic oscillators has been made by Bohigas, Tomsovic, and Ullmo [15]. Among other aspects, these authors have investigated the relation between classical phase space transport (flux through partial barriers) and quantum features such as energy level spacing statistics.

In the present paper we study the classical-quantum correspondence for a system of two quartic oscillators with quartic potential coupling. Our approach is complementary to that of Ref. [15], with a focus on application of semiclassical periodic orbit theory to the study of the evolution of the quantum density of states from the integrable to the strongly coupled limit. For most of the coupling parameter values studied, our system has a generic "mixed" phase space structure [1,18]. Particular emphasis will be given to the manifestations of classical bifurcations in the quantum spectrum [19,20]. For important prior work on bifurcations, see [21–23]. The

issue of wave function localization in the vicinity of periodic orbits [24] is also briefly discussed.

II. THE HAMILTONIAN

We shall investigate the Hamiltonian

$$H = \frac{1}{2}p_1^2 + \frac{1}{2}p_2^2 + \eta_1 q_1^4 + \eta_2 q_2^4 + \gamma q_1^2 q_2^2. \qquad (2.1)$$

It has been much studied previously [8–16], though usually in the limit $\eta_1, \eta_2 \to 0$ (see, e.g., [10,13]). In order to lift the degeneracy between the two oscillators, thereby reducing the symmetry of the model to that of a rectangle (symmetry group D_2), we set $\eta_1 = 1.05$ and $\eta_2 = 0.95$. We then investigate the classical and quantum dynamics as γ is increased from zero up to a "large" value $\gamma = 15$.

Because the Hamiltonian (2.1) is homogeneous in the coordinates $\{q_i\}$, its classical solutions exhibit the *scaling* property [25]. Thus, for each trajectory $(\mathbf{p}_0(t), \mathbf{q}_0(t))$ at energy E_0, there exists a corresponding one at energy E, $(\mathbf{p}(\tau), \mathbf{q}(\tau))$, with

$$\mathbf{p}(\tau) = \left(\frac{E}{E_0}\right)^{\frac{1}{2}} \mathbf{p}_0(t),$$

$$\mathbf{q}(\tau) = \left(\frac{E}{E_0}\right)^{\frac{1}{4}} \mathbf{q}_0(t),$$

$$\tau = \left(\frac{E}{E_0}\right)^{-\frac{1}{4}}. \qquad (2.2)$$

In particular, if a periodic orbit at energy E_0 has action S_0 then the corresponding scaled orbit at any other positive energy E will have action

$$S(E) = \epsilon S_0, \qquad (2.3)$$

where $\epsilon \equiv \left(\frac{E}{E_0}\right)^{\frac{3}{4}}$. Hence, given η_1, η_2, and γ, information on periodic orbits at all energies can be obtained from an analysis at just one energy. In this work we use the reference energy $E_0 = 1.0$.

A hybrid Gear algorithm is used for trajectory integration [26] and a combination of Newton-Raphson and bisection methods [27] is employed to find periodic orbits. In all our trajectory calculations energy is conserved to an accuracy of 10^{-14}; quadruple precision is used to compute the stability exponents of the most unstable orbits.

The quantum mechanical energy levels are found numerically by matrix diagonalization using a symmetry projected (totally symmetric, A_1) direct product basis of quartic oscillator eigenfunctions. The quartic oscillator eigenfunctions are in turn generated by diagonalization of the primary mode quartic oscillator Hamiltonians in one-dimensional harmonic oscillator basis sets, with the harmonic frequency chosen to minimize the trace of the Hamiltonian matrix [10]. In Ref. [10] an improvement in convergence was obtained when the basis set was rotated by $\frac{\pi}{4}$; because of the lower symmetry of our system, however, we do not apply this method here. The lowest 1000 energy levels of A_1 symmetry were obtained over the range $0 \leq \gamma \leq 15$.

III. THE INTEGRABLE LIMIT

With the chosen parameters η_1 and η_2, the system Eq. (2.1) is only completely integrable for $\gamma = 0$. Although a system of two uncoupled quartic oscillators is in principle trivial, a semiclassical analysis of the density of states $\rho(E)$ exhibits several interesting features that merit discussion.

For $\gamma = 0$ the classical phase space is entirely filled with invariant tori supporting either quasiperiodic trajectories or one-parameter families of periodic orbits. At the extreme points of phase space lie the two "primary" oscillator orbits: the $i = 1$ primary orbit refers to the periodic orbit in which all the energy is in mode 1, i.e., $p_2 = q_2 = 0$ for all t, and similarly the $i = 2$ primary orbit has $p_1 = q_1 = 0$ for all time. These orbits exist for all values of γ.

Berry and Tabor have expressed the semiclassical density of states for integrable systems in terms of the *rational* (periodic) tori [28]. We now give a brief summary of their method as applied to our system Eq. (2.1). In the zero coupling limit, the quartic oscillator Hamiltonian is separable, i.e.,

$$H = \frac{1}{2}p_1^2 + \frac{1}{2}p_2^2 + \eta_1 q_1^4 + \eta_2 q_2^4 = \alpha_1 I_1^{\frac{4}{3}} + \alpha_2 I_2^{\frac{4}{3}}, \quad (3.1)$$

where $\alpha_i = \left(\frac{3\pi}{4K}\right)^{\frac{4}{3}} \eta_i^{\frac{1}{3}}$ and K is the complete elliptic integral $K = F(\frac{\pi}{2}, \frac{1}{\sqrt{2}}) \simeq 1.85$ [29]. Frequencies are $\omega_i = \frac{\partial H}{\partial I_i} = \frac{4}{3}\alpha_i I_i^{\frac{1}{3}}$.

Using standard Einstein-Brillouin-Keller quantization [28], the semiclassical density of states $\rho(E)$ is

$$\rho(E) = \sum_{\mathbf{n}} \delta(E - H(I_1 = (n_1 + \tfrac{1}{2})\hbar, I_2 = (n_2 + \tfrac{1}{2})\hbar)), \quad (3.2)$$

where the Maslov index is $\frac{1}{2}$ for both oscillators [28]. The sum over the lattice of non-negative integer quantum numbers $\mathbf{n}$ is transformed to a sum of integrals in reciprocal $\mathbf{M}$ space via the Poisson sum formula to give [28]

$$\rho(E) = \frac{1}{\hbar^2} \sum_{\mathbf{M}} e^{-i\pi(m_1 + m_2)}$$

$$\times \int\int e^{\frac{2\pi i}{\hbar}\mathbf{M}\cdot\mathbf{I}} \delta(E - H(\mathbf{I})) dI_1 dI_2. \quad (3.3)$$

The term in Eq. (3.3) with $\mathbf{M} = \mathbf{0}$ is the Thomas-Fermi (TF)density of states [cf. Eq. (4.2)]. To facilitate evaluation of the remaining terms in (3.3) by stationary phase, we use the coordinate system introduced by Berry and Tabor [28]. Define ξ_0 to be the distance along the energy contour from the point in action space $\mathbf{I}$ and let the orthogonal coordinate be ξ_1. We define two normalized vectors: $\mathbf{v}_\perp$, which points in a direction normal to the energy contour, and $\mathbf{v}_\parallel$, which points along the energy contour. We have

$$\mathbf{v}_\perp \propto \left(\frac{\partial H}{\partial I_1}, \frac{\partial H}{\partial I_2}\right) = \frac{1}{(\omega_1^2 + \omega_2^2)^{\frac{1}{2}}}(\omega_1, \omega_2),$$

$$\mathbf{v}_\parallel \propto \left(\frac{\partial H}{\partial I_2}, -\frac{\partial H}{\partial I_1}\right) = \frac{1}{(\omega_1^2 + \omega_2^2)^{\frac{1}{2}}}(\omega_2, -\omega_1), \quad (3.4)$$

and

$$d\mathbf{I} = \mathbf{v}_\perp d\xi_0 + \mathbf{v}_\parallel d\xi_1. \quad (3.5)$$

Using coordinates $\{\xi_i\}$, the nonzero $\mathbf{M}$ terms of Eq. (3.3) become

$$\rho_{\mathbf{M}}(E) = \frac{1}{\hbar^2} \int e^{\frac{2\pi i}{\hbar}\mathbf{M}\cdot\mathbf{I}(\xi_1)} d\xi_1 \int \frac{\delta(\xi_0)}{\left|\frac{\partial H}{\partial \xi_0}\right|} d\xi_0$$

$$= \frac{1}{\hbar^2} \int e^{\frac{2\pi i}{\hbar}\mathbf{M}\cdot\mathbf{I}(\xi_1)} \frac{d\xi_1}{|\omega(\mathbf{I})|}. \quad (3.6)$$

Standard stationary phase arguments are now used to perform this integral [28]. The dominant contributions to the integral come from the vicinity of ξ_1 values satisfying the condition

$$\mathbf{M} \cdot \frac{d\mathbf{I}}{d\xi_1} = m_1 \frac{dI_1}{d\xi_1} + m_2 \frac{dI_2}{d\xi_1} = 0. \qquad (3.7)$$

Using Eq. (3.4), (3.7) gives the stationarity condition

$$m_1 \omega_2 - m_2 \omega_1 = 0, \qquad (3.8)$$

which is a condition for resonance between the two oscillators.

Expanding $\mathbf{M} \cdot \mathbf{I}(\xi_1)$ about $\mathbf{I}^r$, the value of $\mathbf{I}(\xi_1)$ for which resonance occurs (where $\xi_1 = 0$), we have

$$\mathbf{M} \cdot \mathbf{I}(\xi_1) = \mathbf{M} \cdot \mathbf{I}^r + \frac{1}{2}\xi_1^2 \, \mathbf{M} \cdot \frac{\partial^2 \mathbf{I}}{\partial \xi_1^2} + \cdots . \qquad (3.9)$$

From (3.4), the second derivatives are

$$\frac{\partial^2 I_1}{\partial \xi_1^2} = -\omega_1 \frac{\left(\omega_2^2 \omega_1' + \omega_1^2 \omega_2'\right)}{\left(\omega_1^2 + \omega_2^2\right)^2} \qquad (3.10a)$$

and

$$\frac{\partial^2 I_2}{\partial \xi_1^2} = -\omega_2 \frac{\left(\omega_2^2 \omega_1' + \omega_1^2 \omega_2'\right)}{\left(\omega_1^2 + \omega_2^2\right)^2} \qquad (3.10b)$$

$\left(\frac{\partial \omega_i}{\partial I_j} = \delta_{ij}\omega_i'\right)$. Inserting the expansion (3.9) into Eq. (3.6) gives

$$\rho_{\mathbf{M}}(E) = \frac{1}{\hbar^2} \frac{e^{\frac{2\pi i}{\hbar}\mathbf{M} \cdot \mathbf{I}^r}}{|\omega(\mathbf{I})|}$$
$$\times \int_\alpha^\beta d\xi_1 \exp\left\{ \frac{2\pi i}{\hbar} \left[(m_1\omega_1 + m_2\omega_2) \right.\right.$$
$$\left.\left. \times \frac{\left(\omega_2^2 \omega_1' + \omega_1^2 \omega_2'\right)}{\left(\omega_1^2 + \omega_2^2\right)^2} \right] \frac{\xi_1^2}{2} \right\}. \qquad (3.11)$$

Although the limits of this integration should strictly be the limits of the energy contour (i.e., where the energy contour intersects the $I_1 = 0$ and $I_2 = 0$ axes), we assume that $\hbar$ is small enough so that we may take $\alpha = -\infty$ and $\beta = +\infty$. Note that this assumption is not valid for the $m_1 = 0$ or $m_2 = 0$ resonances, as they lie exactly on the $I_2 = 0$ or $I_1 = 0$ axes. A special treatment of these resonances is given below.

Carrying out the integration by stationary phase yields

$$\rho(E) = \rho_{\mathrm{TF}}(E) + \frac{2}{\hbar^{\frac{3}{2}}} \sum_{\mathbf{M}} e^{-i\pi(m_1+m_2)} A_{m_1 m_2} e^{\frac{2\pi i}{\hbar}\mathbf{M} \cdot \mathbf{I}^r} e^{\frac{i\pi}{4}}, \qquad (3.12)$$

where

$$A_{m_1 m_2} = \left\{ \frac{\left(\omega_1^2 + \omega_2^2\right)}{\left(m_1\omega_1 + m_2\omega_2\right)\left(\omega_2^2 \omega_1' + \omega_1^2 \omega_2'\right)} \right\}^{\frac{1}{2}} \qquad (3.13)$$

and $\mathbf{M}$ is summed over all two-dimensional integer vectors with both components positive and nonzero. The factor of 2 arises because we actually need to sum over the $(-,-)$ as well as the $(+,+)$ quadrant as the resonance condition can be satisfied in both of these quadrants.

By substituting the expressions for the frequencies $\{\omega\}$ and their derivatives $\{\omega'\}$ into (3.13) and using the scaling relation (2.3), we find that $A_{m_1 m_2} \propto E^{\frac{1}{8}}$. Note that this implies a different scaling of the premultiplying factor to that obtained in the classically hard chaotic case (cf. Sec. IV).

As $\mathbf{M} \cdot \mathbf{I}^r \propto E^{\frac{3}{4}}$, we can write (3.12) in terms of the reduced energy ϵ:

$$\rho(\epsilon) = \rho_{\mathrm{TF}}(\epsilon) + \frac{2}{\hbar^{\frac{3}{2}}} \sum_{\mathbf{M}} e^{-i\pi(m_1+m_2)}$$
$$\times A_{m_1 m_2}^0 \epsilon^{\frac{1}{8}} e^{\frac{2\pi i}{\hbar}\mathbf{M} \cdot \mathbf{I}_0^r \epsilon} e^{\frac{i\pi}{4}}. \qquad (3.14)$$

In the zero coupling limit, all terms in (3.14) can be calculated analytically. In Fig. 1 we show the Fourier transform of the density of states (times the factor $\epsilon^{-\frac{1}{8}}$) as obtained by matrix diagonalization compared with the analytical result of Eq. (3.14). It can be seen that the positions of the peaks are well predicted, but the amplitudes follow the predicted pattern only approximately. Inclusion of contributions from complex closed orbits [28] would presumably improve agreement between numerical and theoretical results.

We have already mentioned one problem with the stationary phase evaluation of the contribution to the integral from the $(m_1, 0)$ and $(0, m_2)$ resonances. A more fundamental problem arises because the Taylor expansion about the stationary point breaks down for these resonances. In the case $\mathbf{M} = (m_1, 0)$, the stationarity condition for the integral (3.6) is $m_1 \frac{dI_1}{d\xi_1} = 0$. Because $\frac{dI_1}{d\xi_1} = \omega_2 \left(\omega_1^2 + \omega_2^2\right)^{-\frac{1}{2}}$, this implies that $\omega_2 = 0$ and $I_2 = 0$. This in turn means that $\omega_2' = \infty$ and so the Taylor expansion about the point $I_2 = 0$ does not exist. However, as $v_\perp = (1, 0)$ and $v_\parallel = (0, 1)$ for the $(m_1, 0)$ resonance, locally $\xi_1 = I_2$. Rearranging the original Hamiltonian gives

$$I_1 = \left[\frac{\left(H - \alpha_2 I_2^{\frac{4}{3}}\right)}{\alpha_1} \right]^{\frac{3}{4}} = I_1^0 \left[1 - \frac{\alpha_2}{\alpha_1} \left(\frac{I_2}{I_1^0}\right)^{\frac{4}{3}} \right]^{\frac{3}{4}}, \qquad (3.15)$$

with $I_1^0 = \left(\frac{H}{\alpha_1}\right)^{\frac{3}{4}}$. We now assume that $\hbar$ is sufficiently small that the dominant contribution to (3.6) comes from the region close to the stationary point and that outside the range $I_2 \ll I_1^0$ the oscillations in the integrand quickly cancel. We can then expand (3.15) using the binomial expansion to give

$$I_1 = I_1^0 \left\{ 1 - \frac{3}{4} \left[\frac{\alpha_2}{\alpha_1} \left(\frac{I_2}{I_1^0}\right)^{\frac{4}{3}} \right] \right.$$
$$\left. - \frac{3}{32} \left[\frac{\alpha_2}{\alpha_1} \left(\frac{I_2}{I_1^0}\right)^{\frac{4}{3}} \right]^2 - \cdots \right\}. \qquad (3.16)$$

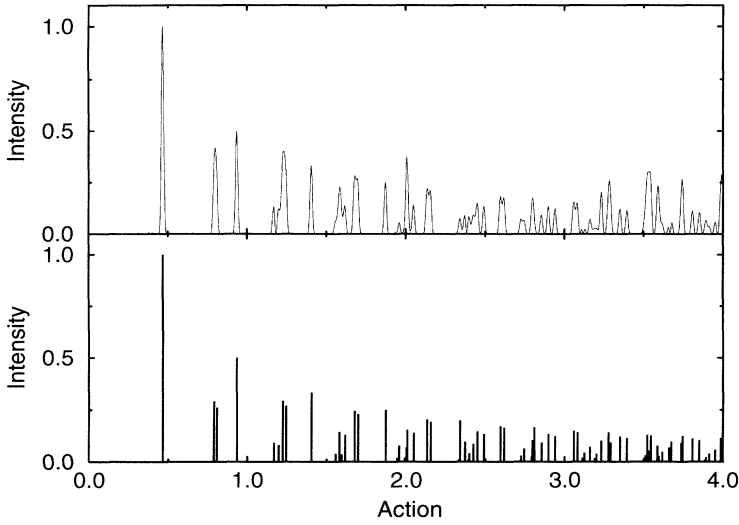Inserting the first two terms of this expression into (3.6), we obtain

FIG. 1. Comparison of the analytical (lower) and numerical (upper) power spectra of the quantum density of states (Fourier transform with respect to the reduced energy ϵ) for $\gamma = 0$. Units of intensity are arbitrary; the height of the largest peak is scaled to unity in both plots.

$$\rho_{\mathbf{M}}(E) = \frac{1}{\hbar^2} e^{\frac{2\pi i m_1 I_1^0}{\hbar}} \frac{2}{|\omega(\mathbf{I})|} \int_0^\infty dI_2 e^{-\frac{2\pi i}{\hbar} m_1 I_1^0 \frac{3}{4} \frac{\alpha_2}{\alpha_1} \left(\frac{I_2}{I_1^0}\right)^{\frac{4}{3}}},$$

$$(3.17)$$

where the upper limit for the integral has been taken to be infinity. Equation (3.17) can be transformed to

$$\rho_{\mathbf{M}}(E) = \frac{1}{\hbar^{\frac{5}{4}}} e^{\frac{2\pi i m_1 I_1^0}{\hbar}} \frac{3}{2|\omega(\mathbf{I})|} \left(\frac{3\alpha_2}{2\alpha_1}\pi m_1\right)^{-\frac{3}{4}} I_1^{0\frac{1}{4}}$$

$$\times \int_0^\infty dx \frac{1}{x^{\frac{1}{4}}} e^{-ix}, \qquad (3.18)$$

where the integral over x is independent of $\hbar$ (and also any other parameter of the Hamiltonian) and finite. Thus the contribution to the density of states from resonances of the form $(m_1, 0)$ [and similarly $(0, m_2)$] goes as $\hbar^{-\frac{5}{4}}$ for

small $\hbar$, whereas the contributions from resonances with both integers nonzero go as $\hbar^{-\frac{3}{2}}$. As we move into the small $\hbar$ regime, for instance, by increasing the energy, the relative magnitude of the contribution of the $(m_1, 0)$ and $(0, m_2)$ terms should therefore decrease. This result is illustrated in Fig. 2, which shows the relative intensity of peaks in the Fourier transform of the numerical density of states at the actions of the 1:0, 0:1 (around $S = 0.38$), and 1:1 (around $S = 0.46$) resonant periodic orbits for the first 200, 500, and 1000 states. As the number of states is increased, the resolution of peak actions improves, but the relative importance of the 1:0 and 0:1 peaks decreases as the effective value of $\hbar$ decreases.

It is interesting to note that the $\hbar^{-\frac{5}{4}}$ dependence of the $(m_1, 0)$ and $(0, m_2)$ terms is intermediate between that of the contribution from real closed orbits with both integers nonzero $(\hbar^{-\frac{3}{2}})$ and that of *complex* closed orbits $(\hbar^{-1})$ [28].
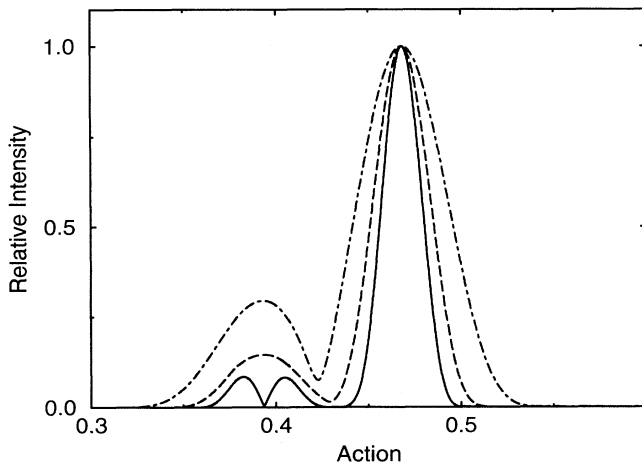
IV. THE STRONG COUPLING LIMIT

In the limit $\gamma \to \infty$ (the $x^2 y^2$ potential [10]), the classical coupled quartic system is almost, but not quite, entirely chaotic; certain stable periodic orbits have been found [13] in this limit, but the size of the regular region about them is very small. As γ becomes larger, calculation of quantum eigenenergies via matrix diagonalization becomes difficult [10] and so we truncate our investigation at the "large" value $\gamma = 15$. At this point the classical dynamics appears to be very largely chaotic (as determined via the Poincaré section), but certain stable periodic orbits remain. In the hard chaotic limit, the semiclassical density of states is expressed in terms of the properties of isolated unstable classical periodic orbits via the Gutzwiller trace formula [1]

$$\rho(E) = \bar{\rho}(E) + \rho^{\mathrm{osc}}(E), \qquad (4.1)$$

where $\bar{\rho}(E)$, the Thomas-Fermi term, is [1]

FIG. 2. Power spectrum of the density of states (with respect to the reduced energy ϵ) for the first 200 (dot-dashed line), 500 (dashed line), and 1000 levels (solid line), at zero coupling. Periodic orbit half actions are 0.39 (1:0 resonant orbit), 0.40 (0:1 resonant orbit), and 0.46 (1:1 orbit).

$$\bar{\rho}(E) = \frac{1}{(2\pi\hbar)^2} \int d\mathbf{p} d\mathbf{q} \, \delta(E - H(\mathbf{p}, \mathbf{q})), \qquad (4.2)$$

and $\rho^{\text{osc}}(E)$ involves a sum over primitive periodic orbits p and their repetitions:

$$\rho^{\text{osc}}(E) = \sum_p \sum_{n=1}^{\infty} \frac{T_p(E)}{\pi\hbar\sqrt{|\text{Det}(M_p^n - \underline{1})|}}$$

$$\times \cos\left\{n\left[\frac{2\pi S_p(E)}{\hbar} - \frac{\pi}{2}\nu_p\right]\right\}. \qquad (4.3)$$

From Eq. (2.3), it can be seen that the Fourier transform of the density of states with respect to the reduced energy ϵ provides information on the actions of the classical periodic orbits contributing to the density of states via (4.3). The stability or monodronomy matrix M_p is independent of energy, as is the index ν_p, so that the energy dependence of the premultiplying term resides in that of the classical period $T_p(E) = T_p(E = 1)E^{-\frac{1}{4}}$. The computed density of states is therefore multiplied by $E^{\frac{1}{4}}$ before Fourier transforming. Because the quantum density of states is available only over a finite energy range, we also multiply by a Blackman-Harris windowing function to reduce "ringing" around peaks [30].

Equation (4.3) gives an expression for the density of states including states of all symmetries in the group D_2. However, because we shall only investigate the totally symmetric (A_1) states, the appropriate symmetry projected form of the density of states must be used [10,31]. Consider the usual formula for the Green function in terms of the quantum eigenstates $|\phi_j\rangle$ [1]:

$$G(q'', q'; E) = \sum_{j=0}^{\infty} \frac{\phi_j(q'')\phi_j^*(q')}{E - E_j}. \qquad (4.4)$$

The definition of an analogous symmetry projected Green function is [10]

$$G^{A_1}(q'', q'; E) = \frac{1}{4} \sum_{\Gamma} G(q'', \Gamma(q'); E) \qquad (4.5a)$$

$$= \frac{1}{4} \sum_{j=0}^{\infty} \frac{1}{E - E_j} \sum_{\Gamma} \phi_j(q'')\phi_j^*(\Gamma(q')), \qquad (4.5b)$$

where the sum is over all symmetry operations Γ under which the Hamiltonian is invariant [i.e., the identity, the two reflections $\Gamma_{\sigma_1}(p_1, q_1, p_2, q_2) = (-p_1, -q_1, p_2, q_2)$ and $\Gamma_{\sigma_2}(p_1, q_1, p_2, q_2) = (p_1, q_1, -p_2, -q_2)$, and the rotation $\Gamma_{C_2}(p_1, q_1, p_2, q_2) = (-p_1, -q_1, -p_2, -q_2)$]. Only eigenstates that are themselves of A_1 symmetry will contribute to this symmetrized Green function.

In taking the trace of (4.4) in the coordinate representation, the stationary phase approximation leads us to consider only those points $\mathbf{q}$ such that $S(\mathbf{q}, \mathbf{q}; E)$, the action of a closed orbit from $\mathbf{q} \to \mathbf{q}$, is stationary with respect to changes $\delta\mathbf{q}$. Hence

$$\frac{\partial S}{\partial \mathbf{q}} = \frac{\partial S}{\partial \mathbf{q}^{\text{final}}}\bigg|_{\mathbf{q}^{\text{final}} = \mathbf{q}} + \frac{\partial S}{\partial \mathbf{q}^{\text{initial}}}\bigg|_{\mathbf{q}^{\text{initial}} = \mathbf{q}}$$

$$= \mathbf{p}^{\text{final}} - \mathbf{p}^{\text{initial}} = 0, \qquad (4.6)$$

establishing that only *periodic* orbits need be considered. Similarly, in taking the trace of (4.5a) the stationarity condition selects out points $\mathbf{q}$ where

$$\frac{\partial S}{\partial \mathbf{q}} = \frac{\partial S}{\partial \mathbf{q}^{\text{final}}}\bigg|_{\mathbf{q}^{\text{final}} = \Gamma(\mathbf{q})} + \frac{\partial S}{\partial \mathbf{q}^{\text{initial}}}\bigg|_{\mathbf{q}^{\text{initial}} = \mathbf{q}}$$

$$= \Gamma(\mathbf{p}^{\text{final}}) - \mathbf{p}^{\text{initial}} = 0. \qquad (4.7)$$

This means that only trajectories connecting $(\mathbf{q}, \mathbf{p})$ with a symmetry related point $(\Gamma(\mathbf{q}), \Gamma(\mathbf{p}))$ contribute to the symmetry projected the density of states. Such trajectories comprise segments of periodic orbits in the full configuration space [they do not correspond to the complete periodic orbit unless $\Gamma(\mathbf{q}) = \mathbf{q}$]; equivalently, these trajectories are periodic orbits in the fundamental domain [31]. A given periodic orbit therefore makes an oscillatory contribution to the density of states with the action value determined by its symmetry properties as follows (cf. Fig. 3).

(a) *Self-retracing orbits with full A_1 symmetry [Fig. 3(a)]*. The only orbits of this form are the two primary oscillator periodic orbits $(q_i = 0, i = 1, 2,$ respectively). In both cases, one of the reflections maps a point on the orbit onto a point halfway around the periodic orbit and the other maps each point on the orbit onto itself. Peaks in the Fourier transform spaced at *half* the action of the primary oscillator orbits are expected.

(b) *Self-retracing orbits with one symmetry [e.g., rotation by π as in Fig. 3(b)]*. In this case there is a symmetry operation that maps any point $\mathbf{q}$ on the periodic orbit onto the point halfway around that orbit. Hence, in addition to peaks in the Fourier transform at multiples of the full action of the periodic orbit, peaks at half integer multiples of the orbit action are expected.

(c) (*Self-retracing orbits with no other symmetries [Fig. 3(c)]*. These orbits give rise to peaks in the power spectrum of the A_1 density of states at multiples of the full action only because there is no symmetry operation that maps a point on the periodic orbit to another on that orbit, except the identity. [Note that our quartic potential has $\eta_1 \neq \eta_2$, so that the orbit in Fig. 3(c) is *not* symmetric with respect to reflection in the diagonal $q_1 = q_2$.]

(d) *Non-self-retracing orbits with full A_1 symmetry [Fig. 3(d)]*. In this case, there is a symmetry operation that maps all $\mathbf{q}$ on the periodic orbit onto the corresponding point half way around the orbit. Thus there will be peaks in the Fourier transformed A_1 density of states at half multiples of the action.

(e) *Non-self-retracing orbits with one symmetry (e.g., one rotation) [Fig. 3(e)]*. In this case the action along the periodic orbit from $\mathbf{q}$ to $\Gamma(\mathbf{q})$, where Γ is the reflection under which the orbit is invariant, will vary along the orbit. This means that the only stationary contribution to $g^{A_1}(E)$ comes from the full action around the orbit and so these orbits will only contribute to the Fourier
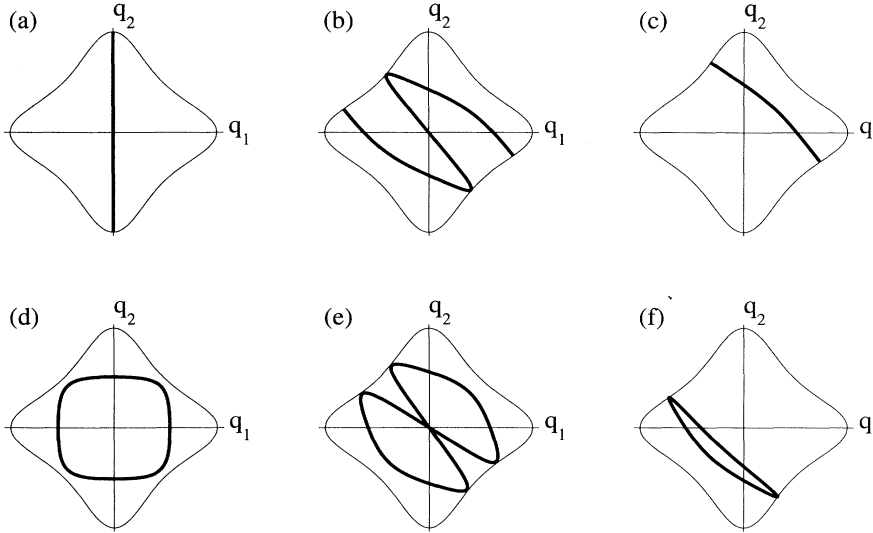
FIG. 3. Periodic orbits of the six symmetry types discussed in the text. Note that the potential is not symmetric under reflection through the line $q_1 = q_2$.

transform of the A_1 density of states with the full action.

(f) *Non-self-retracing orbits with no symmetry* [*Fig. 3(f)*]. These orbits have no symmetry related pairs of points $\mathbf{q}$ and $\Gamma(\mathbf{q})$ apart from $\Gamma = I$ and so the only contribution to $g^{A_1}(E)$ is at the full action $S(\mathbf{q}, \mathbf{q})$.

V. TRANSITION FROM THE CLASSICALLY REGULAR REGIME TO THE CLASSICALLY CHAOTIC REGIME

A. Classical mechanics

The evolution of the phase space structure of the system (2.1) with changes in the coupling parameter γ is illustrated in Fig. 4, which shows Poincaré sections (sectioning condition $p_2 = 0$, $\dot{p}_2 > 0$) for several values of γ. For each value of γ, we propagate the stable and unstable manifolds [18] of any of the following periodic orbits that are unstable: the two primary oscillator modes (of these, the $i = 2$ mode intersects the Poincaré section at $p_1 = q_1 = 0$ for all values of γ, whereas the $i = 1$ mode, having $p_2 = 0$ along its length, lies along the energy boundary of the Poincaré section, leading to an unusual form for the stable and unstable manifolds), the *diagonal* orbits, and the *circular* orbits. Note that the diagonal orbits always lie on the symmetry line $p_1 = 0$ and the circular orbits always lie on the line $q_1 = 0$.

For the zero coupling, integrable case (not illustrated), the entire Poincaré section is filled with invariant curves corresponding to invariant tori surrounding the $i = 2$ primary orbit (at $p_1 = q_1 = 0$). Among these tori are the rational tori covered by one-parameter families of periodic orbits. The lowest-order rational torus corresponds to the 1:1 resonance and both the diagonal and circular orbits lie on this torus.

Upon addition of a small nonintegrable perturbation ($\gamma \neq 0$), the resonant tori will in general break up into pairs of stable and unstable orbits [18]. In the case of the 1:1 resonant torus the diagonal orbits become unstable and the circular orbits stable. Figure 4 shows that, as the regular regions around the circular orbits grow in size

with increasing γ, the regular regions around the primary orbits shrink.

As the value of γ is increased towards $\gamma = 2\eta_2 = 1.9$, the diagonal orbits move in towards the $i = 2$ primary orbit dragging their manifolds with them. At $\gamma = 1.9$ the diagonal orbits merge in an inverse symmetric isochronous bifurcation with the $i = 2$ primary orbit [23,32], which then becomes unstable. In the range $2\eta_2 < \gamma < 2\eta_1 = 2.1$ the phase space is largely filled with tori and broken tori surrounding the circular orbits, with the remaining volume being filled by tori and broken tori around the $i = 1$ primary orbit.

At $\gamma = 2\eta_1 = 2.1$, the diagonal orbits reappear by splitting off from the stable $i = 1$ primary mode, which then becomes unstable. In the range $2\eta_1 < \gamma < 6\eta_2$ both primary orbits are unstable. Note that, because the $i = 1$ primary orbit is actually located on the energy boundary of the Poincaré section, the stable and unstable manifolds of this orbit are asymptotic to the boundary. As γ is increased through this range, the volume of phase space occupied by the regular regions around the circular orbits decreases at the expense of the regular regions around the diagonal orbits.

At $\gamma = 6\eta_2 = 5.7$ the circular orbits merge with the $i = 2$ primary orbit as that orbit becomes stable again. In the range $6\eta_2 < \gamma < 6\eta_1$, the phase space is largely filled by tori surrounding the diagonal orbits with the remaining volume being filled by tori about the $i = 2$ primary orbit.

For $\gamma > 6\eta_1 = 6.3$, both the diagonal and the circular orbits are unstable. Increasing γ further causes the areas of the stochastic regions about each orbit to increase until they overlap and global chaos occurs. As found by Dahlqvist *et al.* [13], the phase space for system (2.1) is never entirely chaotic, even in the limit $\gamma \to \infty$. Analytical expressions for the trace of the monodromy matrix for straight line periodic orbits in homogeneous potentials (i.e., primary and diagonal orbits) have been given by Yoshida [33], who proved that the primary orbits oscillate between stability and instability as $\gamma \to \infty$. Primary orbit i changes between stability and instability (or vice
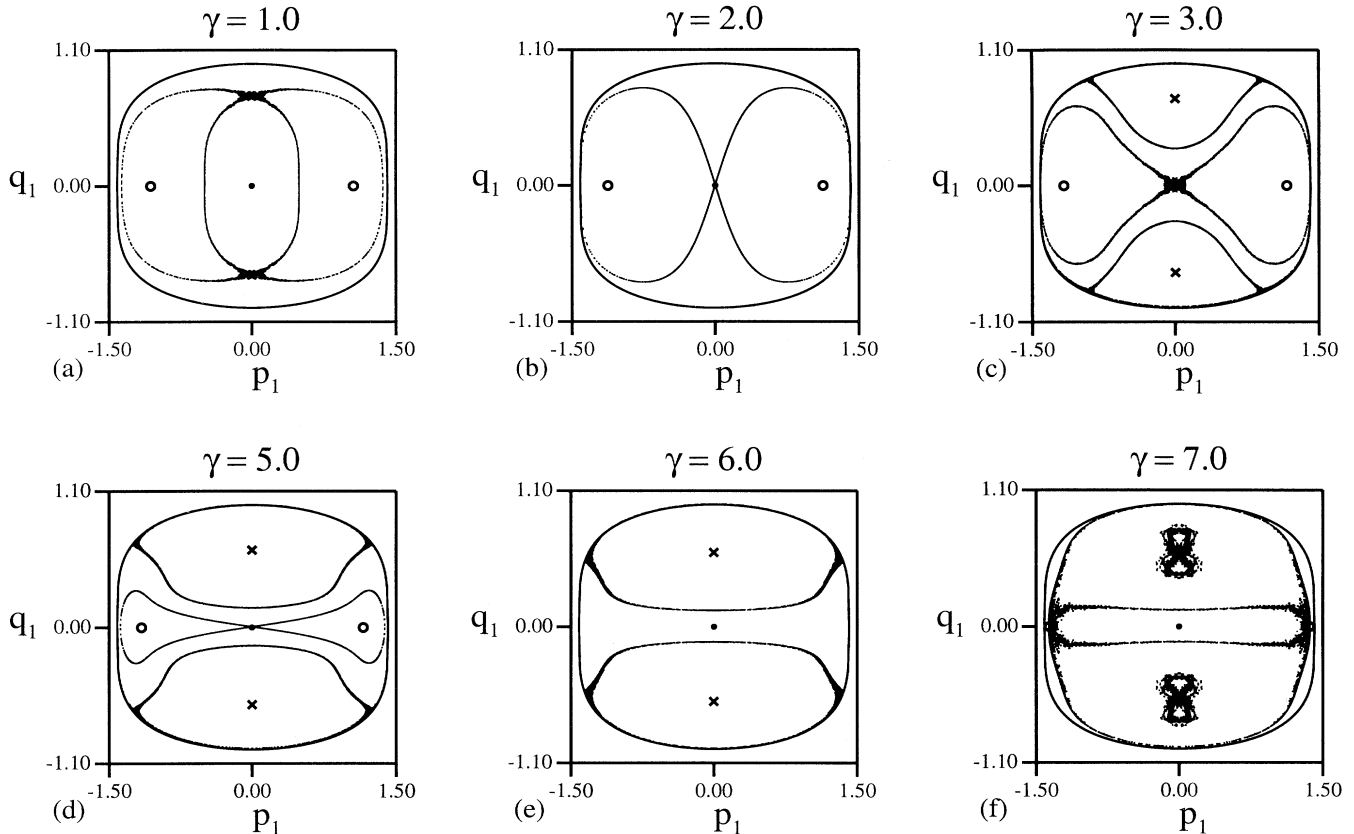
FIG. 4. Classical Poincaré sections (sectioning condition $p_2 = 0$) for different values of γ. Invariant stable and unstable manifolds are shown for the primary, circular, and diagonal periodic orbits, when they are unstable. Symbols for orbits (irrespective of stability): • ($i = 2$ primary mode), ○ (circular orbits), and × (diagonal orbits). (a) $\gamma = 1.0$. (b) $\gamma = 2.0$. (c) $\gamma = 3.0$. (d) $\gamma = 5.0$. (e) $\gamma = 6.0$. (f) $\gamma = 7.0$.

versa) at every point $\gamma = n(n + 1)\eta_i$. We have described the first two of these transitions above. The third such transition also occurs in the range of γ studied, with the simultaneous appearance of 2:1 resonant periodic orbits.

B. The quantum density of states

In the preceding subsection we briefly described the changes in the large-scale classical phase space structure of system (2.1) as the coupling parameter is increased. In Fig. 5 we present a plot of the evolution of the power spectrum of the density of states (Fourier transform with respect to the reduced energy ϵ) as a function of γ. The density of states is calculated by matrix diagonalization at intervals of $\Delta\gamma = 0.1$ and the resulting power spectra are plotted. Each power spectrum has been shifted vertically by an amount proportional to γ. Also plotted in Fig. 5 are the actions of various classical periodic orbits, again as a function of γ. Figure 5 reveals very strikingly the close connection between the classical and quantum dynamics over a range of γ values.

Semiclassical expressions for the density of states were discussed above for both the integrable and hard chaotic

limits [1] and we now investigate the transition between these two limits. Figure 5 shows very clearly the influence of the classical periodic orbit structure on the quantum density of states over the whole coupling parameter range studied. In particular, periodic orbit bifurcations and inverse bifurcations are associated with splittings and mergings of peaks in the power spectrum. Periodic orbit bifurcation sequences in classical Hamiltonian systems are relatively well understood (for two degrees of freedom, at least) [18,21]. An important point is that the primitive semiclassical expression for the density of states, Eq. (4.3), has divergent contributions from bifurcating periodic orbits, when the associated stability matrix M_p or powers thereof has unit eigenvalues [1,19,20]. Ozorio de Almeida and Hannay [20] have given general uniform semiclassical expressions for the contribution of bifurcating periodic orbits, based on the generating function describing the structure of the Poincaré section in the vicinity of the periodic orbit [20]. We have previously applied this method to obtain an analytical form for the semiclassical density of states in the vicinity of a pitchfork bifurcation of the primary oscillator modes in the examples of higher-order resonant bifurcations, for which no analytic form for the parameters in the generat-
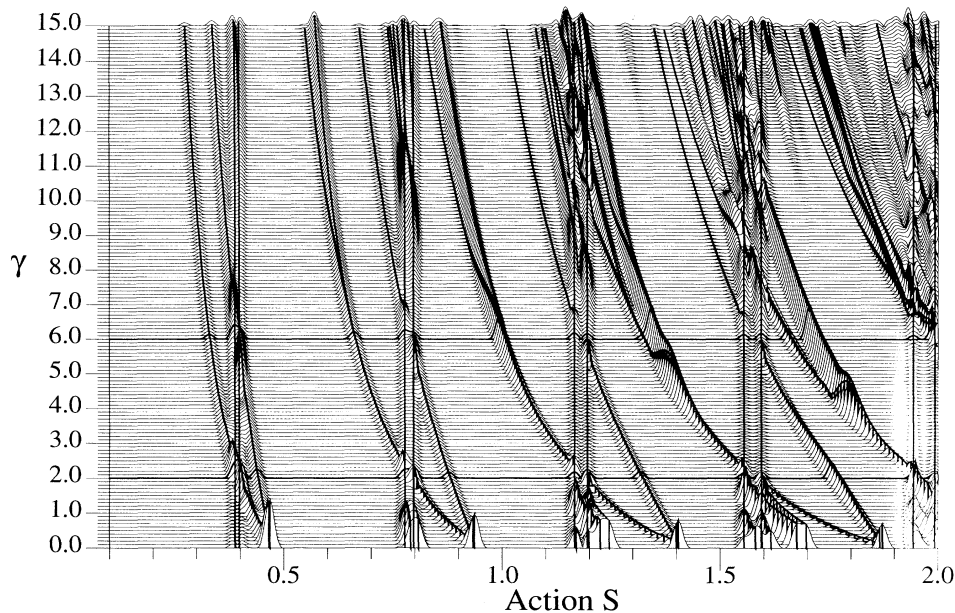
FIG. 5. Power spectrum of the density of states plotted as a function of the coupling parameter γ. Superimposed on this plot are traces of the action or half action (depending upon symmetry) of various classical periodic orbits at $\gamma = E_0 = 1.0$, in units of $\hbar$.

ing function is available, and show how they are manifest in the quantum density of states.

C. Circular orbits

We now investigate the effect of the breakup of resonant tori upon the quantum density of states by following periodic orbits that in the limit of zero coupling lie on the 1:1 resonant torus. There are four such orbits. The two diagonal orbits, which satisfy the condition $q_1 = \alpha q_2$ at all times, were described briefly in [32] and are discussed further below. The initially stable "circular" orbits form simple closed loops enclosing the origin in configuration space; cf. Fig. 6. (For $\gamma = 2\eta_1 = 2\eta_2$, these orbits are exact circles.) The circular orbits exist up to the parameter value $\gamma = 6\eta_2$, at which point they merge with the $i = 2$ primary oscillator mode. At $\gamma = 6\eta_1$, the circular orbits reemerge from the $i = 1$ primary oscillator mode as unstable orbits whose instability increases with γ. This variation of phase space structure with coupling parameter is in certain respects unusual, from the uncoupled integrable case $\gamma = 0$ through the value $\gamma = 2.0$, where the system is nearly separable in terms of radial and angular coordinates, to the point $\gamma = 6.0$, where the system is almost separable in diagonal coordinates.

As γ is increased from zero, the eigenvalues of the monodromy matrix for the circular orbits move around the unit circle towards, but never actually reach, -1 (see Fig. 7). At the same time, the volume of the stable region surrounding the circular orbits increases. As the rotational angle passes through rational multiples of 2π, i.e., $\lambda = e^{\pm 2i\pi \frac{m}{n}}$ with m and n integers, one or two stable-unstable pairs of higher-order periodic orbits are born. At such places the determinant of $|M^n - 1|$ for the nth repetition of the periodic orbit in Eq. (4.3) becomes zero and the stationary phase approximation breaks down.

Following Ozorio de Almeida and Hannay [20], we have given a uniform semiclassical treatment of the density of states through a symmetric pitchfork bifurcation of the primary oscillator modes [32], a case for which an analytical expression for the corresponding generating function $S(\mathbf{q}', \mathbf{q})$ is available. In the vicinity of a general resonant bifurcation, the generating function $S(\mathbf{q}' = \mathbf{q}, \mathbf{q})$ is stationary precisely on the periodic orbits, but the periodic orbits are not isolated on the scale of $\hbar$. Instead of using the stationary phase approximation for each of the periodic orbits individually [that is, assuming a quadratic expansion of $S(\mathbf{q}, \mathbf{q})$ around each orbit], we must use a higher-order expansion, for example, a quartic form
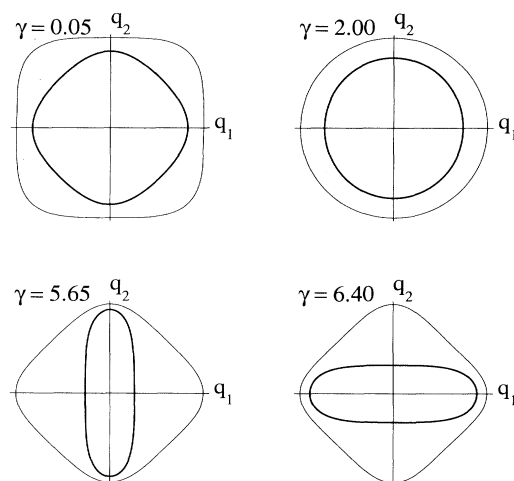

FIG. 6. Evolution of the circular orbits as γ is varied ($E = 1.0$). At $\gamma = 5.7$ the circular orbits merge with the $i = 2$ primary periodic orbit and emerge from the $i = 1$ primary orbit at $\gamma = 6.3$.
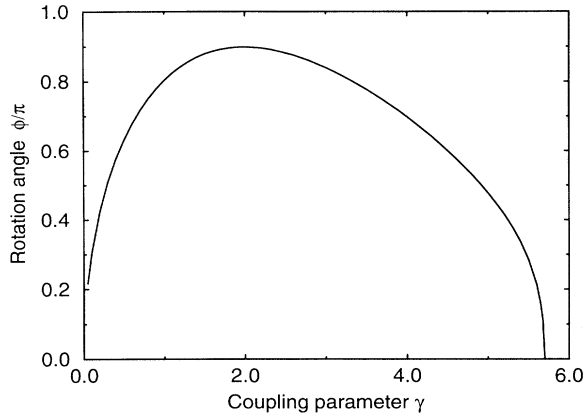
FIG. 7. Rotation angle about the (stable) circular orbit as a function of the coupling parameter γ.

[23,32]. In [32] we were able to derive analytic forms for the coefficients in the symmetric quartic expansion about the central periodic orbit, but in the general case this is not possible. Nevertheless, the results of [32] are useful in that they enable us to understand qualitatively the semiclassical manifestations of the different types of bifurcation leading to the appearance of resonant periodic orbits.

As an example, consider the formation of the 5:12 resonant periodic orbits about the circular orbit (Fig. 8). In the 5 times they loop the origin before closing, each of these resonant periodic orbits undergoes 12 radial oscillations. The 5:12 orbits emerge from the circular orbit at $\gamma = 0.98$ and disappear by merging with it at $\gamma = 3.34$ (cf. the nonmonotonic behavior of the winding number in Fig. 7). There are four of these non-self-retracing orbits, each of which has the full D_2 symmetry of the Hamiltonian and so gives a peak in the Fourier transform of the density of states at half the full action. The actions of the 5:12 orbits are only slightly different from the action of the fifth repetition of the circular orbit itself, the difference being sufficiently small that separate peaks are not resolved in our Fourier transform computed with a finite number of energy levels. In Fig. 9 we show the Fourier transform of the density of states in the vicinity of the half action of the 5:12 orbits. The half action of the 5:12 resonant periodic orbits is indicated as well as 2.5 times the action of the circular orbit. While the multifurcation
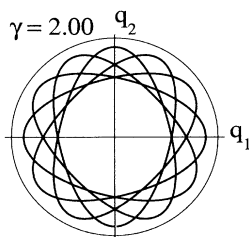

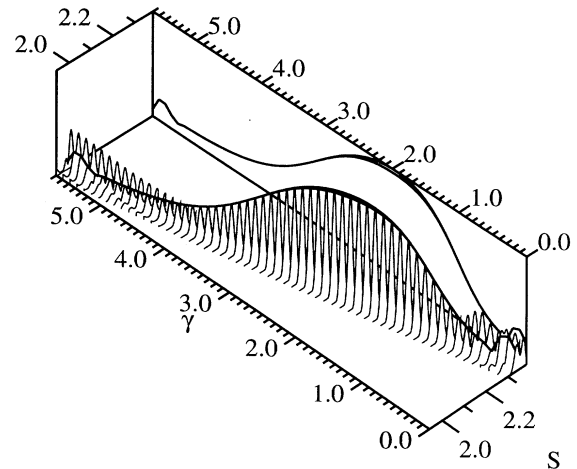FIG. 8. The 5:12 resonant periodic orbit at $\gamma = 2.0$.

FIG. 9. Power spectrum of the density of states as a function of γ. Superimposed upon the peaks are traces at (a) five times the half action of the circular orbits and (b) the half actions of the 5:12 resonant periodic orbit in Fig. 8 (in units of $\hbar$). Also shown (projected onto the back wall) are the peak heights at the actions of the periodic orbits. Note that the action values are very similar. The bifurcation leading to the emergence of the 5:12 periodic orbits occurs at $\gamma = 0.98$ and the bifurcation leading to their disappearance occurs at $\gamma = 3.34$.

leading to the appearance of the resonant orbits is certainly manifest as an increase in the peak height in the vicinity of the corresponding classical parameter value, the maximum peak height is not, however, found at the bifurcation point ($\gamma = 3.34$), but rather on the side of the bifurcation where multiple periodic orbits exist (cf. [32]).

Although other higher-order multifurcations occur around the circular orbits, the new orbits have such high actions that the corresponding peaks in the Fourier transformed density of states overlap with the peaks corresponding to multiple repetitions of lower action periodic orbits. This makes identification of the effect of the multifurcation difficult. We have, however, observed significant enhancement of intensity at actions near the repetitions of the circular orbit for parameter values where the corresponding higher-order periodic orbit emerges.

As stated above, the eigenvalues of the monodromy matrix of the circular orbit do not quite reach -1 before it merges with the $i = 2$ primary mode at $\gamma = 6\eta_2$, so that no period-doubling bifurcation occurs. Accordingly, we do not expect enhancement of peaks at low-order repetitions of the circular periodic action. This is indeed the case for the first, second, and third repetitions of the half action, but the fourth repetition is enhanced (Fig. 10). The reason is that the eigenvalues of the monodromy matrix for the periodic orbit come close to -1 for $\gamma \sim 2.0$ and so the determinant in (4.3) becomes small. If the eigenvalues actually reached -1, a period-doubling bifurcation would occur [18].

At $\gamma = 2.0$ the Hamiltonian (2.1) is almost separable; for $\gamma = 2\eta_1 = 2\eta_2$ it is separable in terms of polar
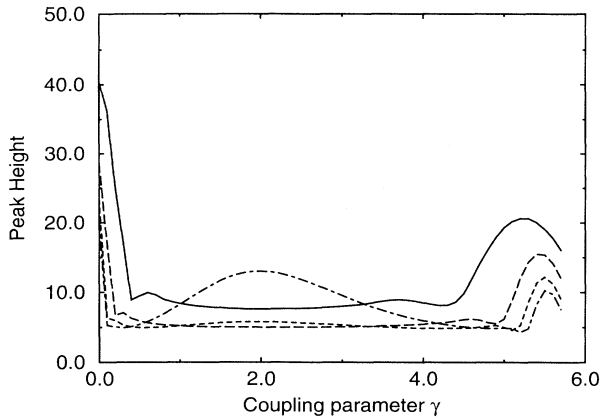
FIG. 10. Peak height in the power spectrum of the quantum density of states at action values corresponding to the first four repetitions of the half action of the circular orbits: first (solid), second (long dashed), third (short dashed), and fourth (chain). Note the enhancement of the intensity at the fourth repetition at $\gamma \simeq 2.0$. Also note the small peaks close to the bifurcation point $\gamma = 5.7$. These correspond to the "supernumerary rainbow peaks" briefly mentioned in [32].

coordinates and torus quantization is again appropriate. However, with our chosen parameters, although most of the phase space is filled with tori around the circular orbits, there is a small region of phase space around the one remaining stable primary oscillator mode; associated peaks appear in the power spectrum of the density of states.

D. Diagonal orbits

The "diagonal" orbits were described in [32]. These orbits, which also lie originally on the 1:1 resonant torus, rotate in configuration space as γ is increased away from zero, until at $\gamma = 2\eta_2$ they merge with the $i = 2$ primary periodic orbit. In [32] we described a uniform semiclassical analysis of the associated inverse pitchfork bifurcation at $\gamma = 2\eta_2$. Another bifurcation at $\gamma = 2\eta_1$ leads to the reemergence of the diagonal periodic orbits out of the $i = 1$ primary periodic orbit.

In the range $0 < \gamma < 2\eta_2$ the diagonal orbits are unstable, but above $\gamma = 2\eta_1$ they are stable, leading to the possibility of resonant and period multiplying bifurcations (described below). First, however, we consider the pitchfork bifurcation that occurs when the eigenvalues of the diagonal orbits again reach $+1$ (at $\gamma \simeq 6.0$). The diagonal orbits become unstable with the production of two new stable periodic orbits of the same period. However, whereas the diagonal orbits do possess one symmetry — they are invariant with respect to a rotation by π about the origin — the new orbits possess no symmetries. Except for a small range of γ, where they are unstable with reflection, these new orbits are stable up to $\gamma \simeq 13.89$ at which point another pitchfork bifurcation occurs. When-

ever the newly produced orbits change from being stable to unstable, new periodic orbits emerge, either of the same period or of double the period according to the sign of the monodromy eigenvalues at the transition. We have followed several of these higher-order periodic orbits as a function of γ (Fig. 11).

The power spectrum of the density of states is shown in Figs. 12 and 13. In the vicinity of action values corresponding to the first occurrence of the diagonal orbit half action (Fig. 12), the peak height monotonically decreases as γ increases. At the full action, however (Fig. 13), the pitchfork bifurcation at $\gamma \simeq 6.0$ is manifest as an increase in peak intensity. Above the bifurcation, the larger peaks are associated with the stable lower symmetry orbits produced by the bifurcation, with the diagonal orbits only giving rise to a small peak. Note that, as before, the maximum intensity is not at the point of bifurcation but rather towards the multiple orbit side. Further away from the bifurcation, the intensity corresponding to these stable orbits again increases, up to the next pitchfork bifurcation.

At $\gamma \simeq 4.80$ the eigenvalues of the monodromy matrix of the diagonal orbits pass through $e^{\pm 2\pi i/3}$ and two pairs of stable-unstable period-tripled orbits are produced. The effect on the Fourier transformed density of states is apparent at action values around the half action of these orbits (they have rotational symmetry and so contribute at their half action) with an increase in intensity above the bifurcation point (Fig. 14).

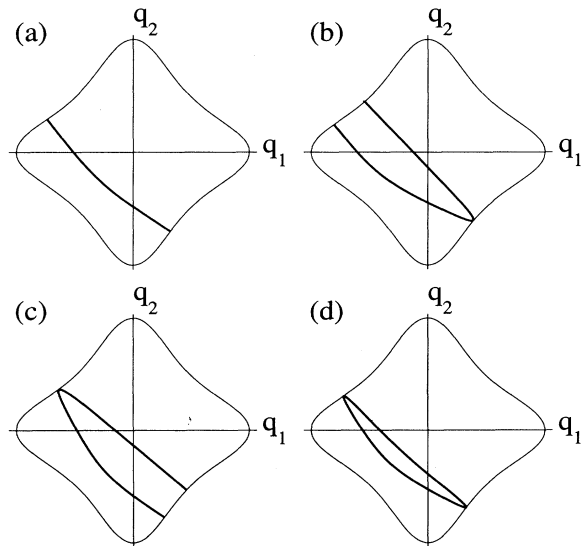At $\gamma \simeq 3.83$ the eigenvalues of the diagonal orbit sta-

FIG. 11. Descendents of the diagonal orbits. All orbits are illustrated at $\gamma = 15.0$. (a) The orbit resulting from the bifurcation at $\gamma \simeq 6.0$. (b) and (c) Orbits emerging from orbit (a) as it briefly becomes unstable with reflection: orbit (b) is born at $\gamma \simeq 7.7$, orbit (c) at $\gamma \simeq 8.3$ (note that these are different orbits because the potential has rectangular symmetry only). (d) The orbit born from (a) at $\gamma \simeq 13.9$. In all these examples we show just one of several symmetry related orbits.
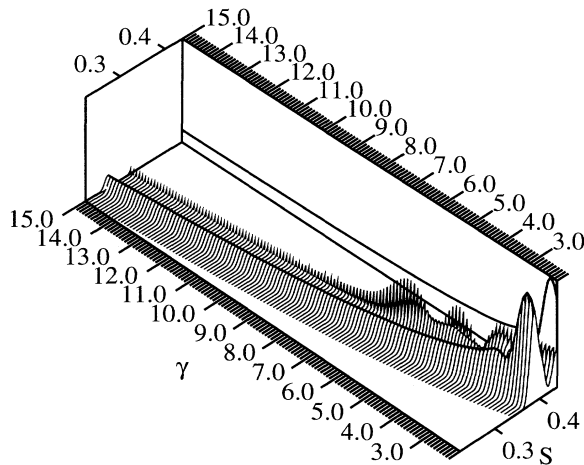
FIG. 12. Power spectrum of the density of states in the vicinity of the half action of the diagonal orbits. Note the monotonic decay of peak height with increasing γ except for the small supernumerary rainbow peak close to the bifurcation point $\gamma = 2.1$. The peaks at actions slightly higher than the diagonal orbits are due to the primary periodic orbits. Actions are in units of $\hbar$.

FIG. 14. Power spectrum of the density of states in the vicinity of three times the half action of the diagonal orbits. The multifurcation of the classical periodic orbit occurs at $\gamma = 4.80$. The larger amplitude in the power spectrum is associated with higher action period-three orbits. Actions are in units of $\hbar$.

bility matrix reach -1 and we observe a period doubling resulting, because of the symmetry, in two unstable self-retracing and two stable non-self-retracing orbits being formed from each diagonal orbit (thereby conserving index). None of the new orbits has any of the spatial symmetries of the Hamiltonian. The diagonal orbits remain stable as the rotation angle increases through π. The quantum manifestation of this period-doubling bifurcation is shown in Fig. 15 (cf. Ref. [32]). The maximum peak intensity is again on the multiple periodic orbit side of the bifurcation and the peak for the higher action periodic orbit has greater intensity than that for the rep-

etition of the shorter orbit. In Fig. 15, the effect of the pitchfork bifurcation illustrated in Fig. 13 is apparent at its second repetition.

E. Saddle-center bifurcations

Mao and Delos have described the creation of "exotic" orbits at saddle-center (tangent) bifurcations [21]. A semiclassical theory for the effect of such bifurcations on the density of states was given by by Kuś et al. [34], who introduced the notion of "ghost" periodic orbits to explain the appearance of peaks in the Fourier transformed
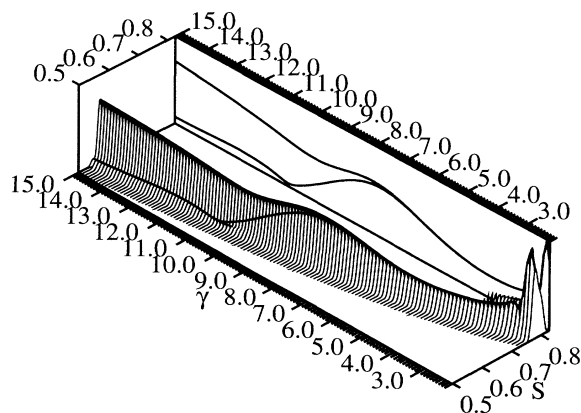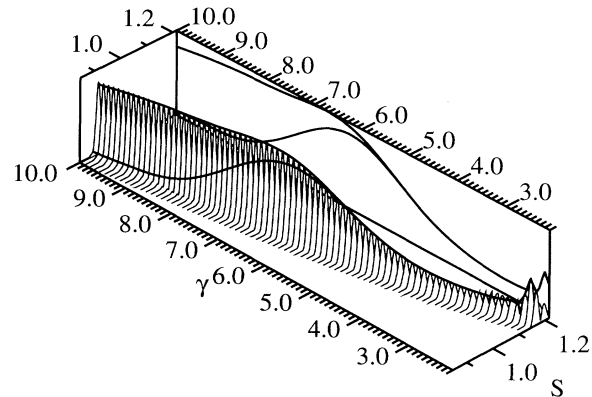

FIG. 13. Power spectrum of the density of states in the vicinity of the full action of the diagonal orbits. The pitchfork bifurcation leading to the lower symmetry orbits occurs at $\gamma \simeq 6.0$. Note that the larger peaks for γ greater than this value are associated with the stable lower symmetry orbits. Actions are in units of $\hbar$.
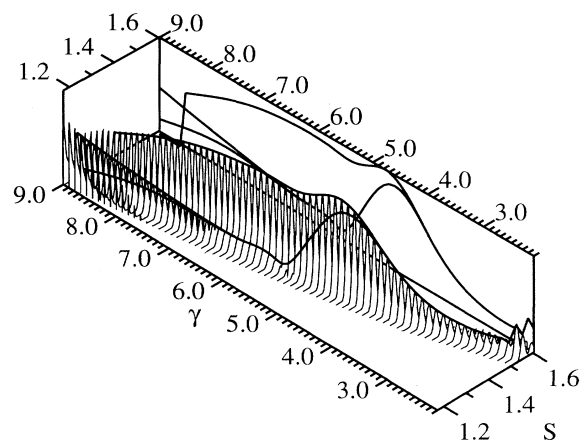

FIG. 15. Power spectrum of the density of states in the vicinity of four times the half action of the diagonal orbits. The bifurcation leading to the appearance of the period-doubled orbits is at $\gamma \simeq 3.8$. Also appearing on this figure (at $\gamma \simeq 6.0$) is the repetition of the pitchfork bifurcation leading to the emergence of the lower symmetry period one orbits. Actions are in units of $\hbar$.

quantum density of states at parameter values for which there was no *real* classical periodic orbit. It is not possible to find orbits produced by tangent bifurcations by systematically following branches of the bifurcation tree from known periodic orbits; rather, because such orbits "appear out of nowhere" (though in pairs), a thorough search at a particular parameter value is necessary to reveal one of these orbits. Once such an orbit is found, it can be followed to smaller values of the coupling parameter until a bifurcation is reached. In the case that the bifurcation is a saddle-center bifurcation, the complementary periodic orbit can then be followed by increasing the coupling parameter. It is important to note that, because of the existence of saddle-center bifurcations it is not possible to guarantee that all periodic orbits with actions below a certain value, say, have been found at a particular γ value.

In a small number of cases, we observe sets of peaks in the Fourier transformed density of states at action values that have no apparent relation to the actions of other, known, periodic orbits. In those cases we have investigated, we find that such peaks are associated with a pair of periodic orbits produced by a saddle-center bifurcation. One pair of such orbits is shown in Fig. 16. The two periodic orbits are self-retracing with one symmetry [the reflection $(p_1, q_1) \rightarrow (-p_1, -q_1)$], so there is a peak in the power spectrum at half the classical action (Fig. 17). It is conceivable that there are other periodic orbits having nearly the same action that we have not found; the match between the position of the peak and the action of the orbits in Fig. 17 is nevertheless quite convincing. As observed in [32], the maximum peak height as a function of coupling parameter occurs not at the bifurcation value itself but towards the side where the real periodic orbits exist. Although a uniform semiclassical treatment of the density of states in terms of Airy functions would be appropriate in this case [34], neither the actions nor the positions in the Poincaré section are known analytically.

It should be pointed out that, although saddle-center bifurcations are not uncommon in the classical dynamics, it is difficult to unambiguously identify their manifestations in the quantum system. In the range of γ values where saddle-center bifurcations occur, there are many other classical periodic orbits with comparable actions and the contributions of these other orbits to the density of states can obscure the effect of the ghost orbits.
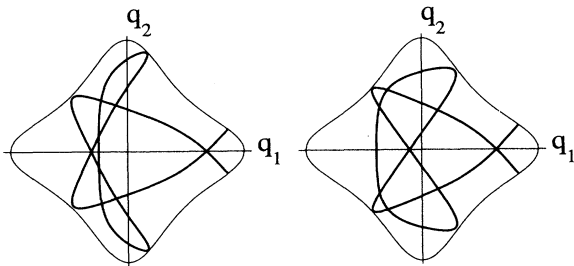

FIG. 16. Pair of periodic orbits appearing at a saddle-center bifurcation at coupling parameter $\gamma \simeq 12.8$.
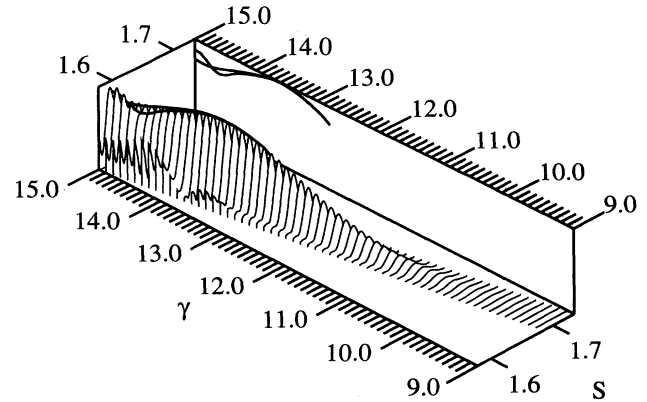

FIG. 17. Manifestation of a classical saddle-center bifurcation in the power spectrum of the quantum density of states. The half actions of the relevant classical periodic orbits are also shown (in units of $\hbar$). The saddle-center bifurcation occurs at $\gamma \simeq 12.8$, below which point the two relevant periodic orbits cease to exist.

F. General comments

We have illustrated the effect of various classical bifurcation phenomena upon the quantum density of states. While it is neither possible nor useful to examine every such bifurcation, we have followed several periodic orbits from their formation through to the upper limit of γ we are able to study quantum mechanically. Many features of the power spectrum of the quantum density of states can be understood in terms of individual classical periodic orbits or small sets thereof, although in many cases the existence of a number of periodic orbits close in action prevents unambiguous assignment. Moreover, because of the occurrence of saddle-center bifurcations, it is not possible to guarantee that all periodic orbits with actions less than a certain value have been found.

VI. EIGENSTATE LOCALIZATION AND PERIODIC ORBITS

Thus far our discussion of system (2.1) has centered on the quantum density of states. There is, however, also considerable current interest in the properties of eigenfunctions of nonintegrable systems [1]. The localization of eigenfunctions in the vicinity of periodic orbits in both configuration space [24] and in phase space [35] has attracted much attention.

We do not give a systematic survey of the eigenstates of system (2.1) in the present paper. In this section we make a number of observations concerning the apparent influence of the most important short (primary, diagonal, and circular) periodic orbits on certain subsets of eigenstates. A discussion of "smoothed" eigenstates [36] is reserved for a later paper.

In Fig. 18 we show the variation of eigenvalues (reduced energies) with γ ($\eta_1 = 1.05$ and $\eta_2 = 0.95$). Clearly present in the correlation diagram are "diabatic states"
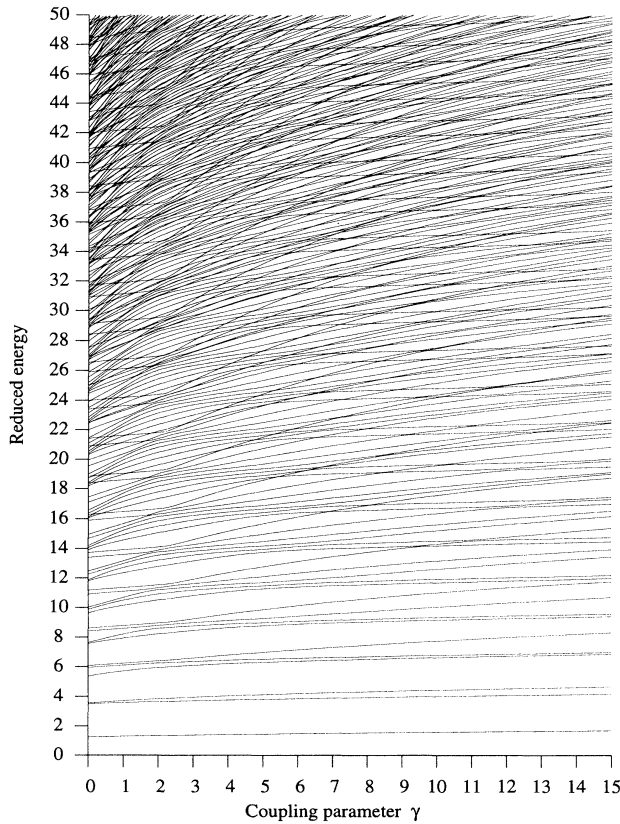
FIG. 18. Correlation diagram showing A_1 symmetry eigen-values as a function of coupling parameter γ. Dimensionless reduced energies $\epsilon = (E/E_0)^{3/4}$ are plotted.

i.e., states whose energies vary smoothly with γ, with only local avoided crossings perturbing them [37].

Notable among the diabatic states are sequences of nearly horizontal lines at large γ values. These dia-batic curves are associated with states that are localized

along the primary mode periodic orbits. Sequences of such states can be identified corresponding to successive excitation of quanta along the primary modes and the energies of such states are well approximated by sim-ple one-dimensional Bohr-Sommerfield quantization con-ditions [11]. In Fig. 19 we show the reduced energies of states localized along the $i = 2$ primary periodic orbit as a function of coupling parameter and quantum num-ber n_2. The relation between reduced energy and quan-tum number is approximately linear, as follows from sim-ple one-dimensional semiclassical quantization [11]. The state energies are moreover approximately independent of the coupling parameter in the range of γ considered. In Fig. 20 we show a sequence of configuration space plots of states localized along the $i = 2$ primary mode for sev-eral γ values, each at energies corresponding to 20 quanta along the primary mode and zero quanta transverse. De-spite the accuracy of the one-dimensional quantization for computation of energies, the eigenstates themselves are subject to the influence of periodic orbits other than the primary orbits. In the last eigenstate of Fig. 20 there is clearly some influence of the "figure eight" orbit also marked.

By following a different diabatic stat state, we can ob-serve the effect of the pitchfork bifurcation of the clas-sical diagonal periodic orbit on the eigenfunctions. In Fig. 21 we show the energy level correlation diagram in the vicinity of the diabatic curve associated with states having 22 nodes along the diagonal orbit and none across it. Because of the symmetry, eigenstates will be scarred by both diagonal orbits and some care is necessary when counting nodes. Configuration space densities and quan-
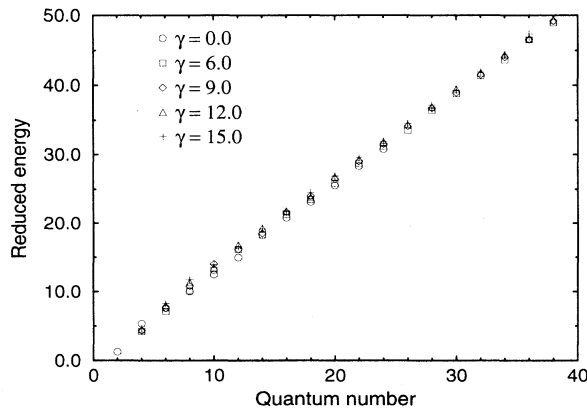

FIG. 19. Reduced energy of the eigenstates localized along the $i = 2$ primary periodic orbit as a function of quantum number and coupling parameter.

(a) $\gamma = 6.0$
No. 52   E = 78.76

(b) $\gamma = 9.0$
No. 50   E = 79.79

(c) $\gamma = 12.0$
No. 48   E = 80.55

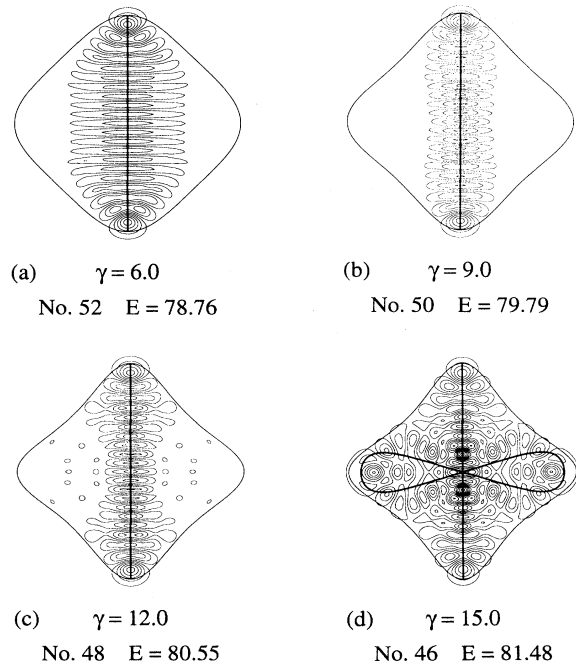(d) $\gamma = 15.0$
No. 46   E = 81.48

FIG. 20. Configuration space plots of eigenstates localized along $i=2$ primary orbit, with $n_2 = 20$ quanta along the orbit. (a) $\gamma = 6.0$. (b) $\gamma = 9.0$. (c) $\gamma = 12.0$. (d) $\gamma = 15.0$.
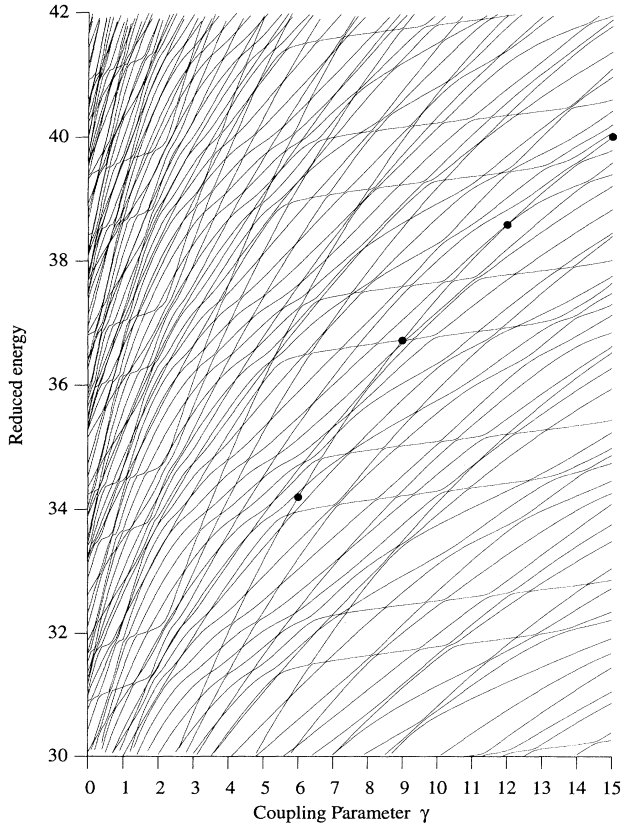
FIG. 21. Portion of the energy versus γ correlation diagram. The dots indicate the states shown in Figs. 22 and 23. Dimensionless reduced energies $\epsilon = (E/E_0)^{3/4}$ are plotted.
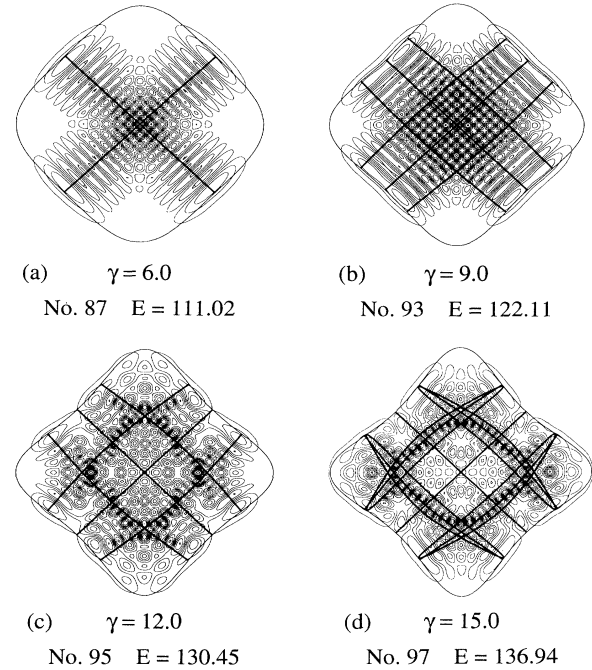

FIG. 22. Configuration space densities for eigenstates localized along the diagonal orbits with $n = 22$ quanta excited along the orbit. The states shown are $\gamma = 6.0$, state 87; $\gamma = 9.0$, state 93; $\gamma = 12.0$, state 95; and $\gamma = 15.0$, state 96 (note that the lowest eigenstate is numbered zero).

tum surfaces of section (Husimi representation [38]) are shown for the indicated eigenstates in Figs. 22 and 23, respectively. The locations of relevant classical periodic orbits are marked in Fig. 23. At $\gamma = 6.0$ the system is almost separable in terms of diagonal coordinates (at $\gamma = 6\eta_1 = 6\eta_2$ the system is exactly separable in these coordinates) and it is easy to recognize eigenstates localized along the diagonal periodic orbit. For a value of $\gamma \simeq 6.007$ the diagonal orbit becomes unstable at a pitchfork bifurcation (as discussed above). The influence of the new stable orbits on the eigenstate at $\gamma = 9.0$ is clear from the spreading of the state in configuration space transverse to the diagonal orbit. The Husimi representation also reveals scarring of the phase space density by the new stable orbits. At $\gamma = 12.0$ the diabatic state is involved in an avoided crossing. However, scarring by descendents of the diagonal orbit is still apparent. The effect of the avoided crossing is manifest in the Husimi representation in the appearance of significant phase space density about the circular periodic orbit. (The circular orbit intersects the section at $q_1 = 0$, $p_1 = \pm 1.356$.) A plot of the other state involved in this avoided crossing (Fig. 24) shows it to be dominated by the circular orbit, as expected. At $\gamma \simeq 13.8$ the new low symmetry orbits become unstable with the simultaneous appearance of two new stable orbits. All these orbits are marked on
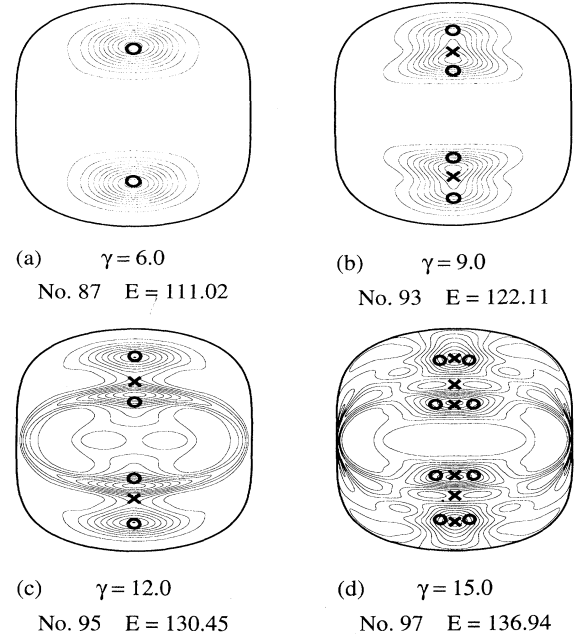

FIG. 23. Quantum surface of section (Husimi representation) for eigenstates localized along the diagonal orbits with $n = 22$ quanta excited along the orbit. The quantum surface of section corresponds to the classical Poincaré section shown in Fig. 4 (i.e., $p_2 = 0.0$). The states shown are: $\gamma = 6.0$, state 87; $\gamma = 9.0$, state 93; $\gamma = 12.0$, state 95; and $\gamma = 15.0$, state 96 (note that the lowest eigenstate is numbered zero). The location of stable ($\circ$) and unstable ($\times$) classical periodic orbits resulting from bifurcation of the diagonal orbits are shown.
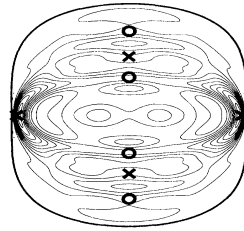
$\gamma = 12.0$

No. 96   E = 130.51

FIG. 24. Quantum surface of section for state 96, which is the other state involved in the avoided crossing with eigenstate number 95 (cf. Figs. 22 and 23) at $\gamma = 12.0$.

the quantum surface of section for the eigenstate along the diabatic state at $\gamma = 15.0$. Because the most recently born orbits are close to their parents in phase space it is not possible to identify unambiguously their influence on the eigenstate.

VII. CONCLUSIONS

In this paper we have investigated the semiclassical mechanics of the coupled quartic oscillator system described by Hamiltonian (2.1). While the almost completely chaotic $q_1^2 q_2^2$ potential (corresponding to the $\gamma \to \infty$ limit) has received much attention, our focus has been on the evolution of the density of states from the integrable case ($\gamma = 0$) to the strongly coupled limit (a large value $\gamma = 15.0$).

For the integrable case, the Berry-Tabor analysis of the semiclassical density of states in terms of rational (peri-

odic) tori [28] is appropriate. We extended this analysis to deal with the contributions of resonances situated at the boundaries of the physical action region. Such resonances have an $\hbar$ dependence intermediate between that for real rational tori and complex periodic tori [28]. It was shown numerically that the magnitudes of the peaks for the (1:0) and (0:1) resonant tori decrease more rapidly with decreasing $\hbar$ than the magnitude of the (1:1) peak.

Computation of power spectra of the quantum density of states for different values of the coupling parameter γ revealed the evolution of the underlying classical periodic orbit structure (cf. [1]), in particular, orbit bifurcations and inverse bifurcations. We were able to identify the influence of several resonant, symmetric isochronous, and tangent bifurcations on the quantum density of states, although it was not possible to determine the parameters appearing in the uniform semiclassical expressions for the contributions to the density of states analytically, as in our previous work [32].

Finally, we briefly discussed localization of eigenstates in the vicinity of the shortest periodic orbits and the manifestations of bifurcations in sequences of eigenstates located along diabatics. A discussion of smoothed states and wave-packet spectra for the present system will be given in a subsequent paper.

ACKNOWLEDGMENTS

[1] M.C. Gutzwiller, *Chaos in Classical and Quantum Mechanics* (Springer-Verlag, Berlin, 1990).

[2] *Chaos and Quantum Physics*, edited by M.J. Giannoni, A. Voros, and J. Zinn-Justin (Elsevier, Amsterdam, 1991); *Quantum Chaos, Proceedings of the International School of Physics* "Enrico Fermi," Course CXIX, Varenna, 1991, edited by G. Casati, I. Guarneri, and U. Smilansky (North-Holland, Amsterdam, 1993).

[3] B. Eckhardt, S. Fishman, K. Müller, and D. Wintgen, Phys. Rev. A **45**, 3531 (1992).

[4] M.L. Du and J.B. Delos, Phys. Rev. A **38**, 1896 (1988); **38**, 1913 (1988); H. Friedrich and D. Wintgen, Phys. Rep. **183**, 37 (1989); G. Alber and P. Zoller, *ibid.* **199**, 231 (1991).

[5] D. Wintgen, K. Richter, and G. Tanner, Chaos **2**, 19 (1992).

[6] J.M. Gomez-Lorente and E. Pollak, Annu. Rev. Phys. Chem. **43**, 91 (1992).

[7] J.M. Gomez-Llorente, S.C. Farantos, O. Hahn, and H.S. Taylor, J. Opt. Soc. Am. B **7**, 1851 (1990).

[8] A. Carnegie and I.C. Percival, J. Phys. A **17**, 801 (1984).

[9] G.K. Savvidy, Nucl. Phys. B **246**, 302 (1984).

[10] B. Eckhardt, G. Hose, and E. Pollak, Phys. Rev. A **39**, 3776 (1989).

[11] V.B. Sheorey, in *Proceedings of the Adriatico Conference on Quantum Chaos*, edited by H.A. Cerdeira, R. Ramaswamy, M.C. Gutzwiller, and G. Casati (World Scientific, Singapore, 1991); S. Sinha and V.B. Sheorey, Mol. Phys. **80**, 1525 (1993).

[12] R.L. Waterland, J.-M. Yuan, C.C. Martens, R.E. Gillilan, and W.P. Reinhardt, Phys. Rev. Lett. **61**, 2733 (1988).

[13] P. Dahlqvist and G. Russberg, Phys. Rev. Lett. **65**, 283 (1990); A.B. Eriksson and P. Dahlqvist, Phys. Rev. E **47**, 1002 (1993).

[14] D. Biswas, M. Azram, Q.V. Lawande, and S.V. Lawande, J. Phys. A **25**, L297 (1992).

[15] O. Bohigas, S. Tomsovic, and D. Ullmo, Phys. Rep. **223**, 43 (1993).

[16] C.C. Martens, R.L. Waterland, and W.P. Reinhardt, J. Chem. Phys. **90**, 2328 (1989).

[17] G.G. de Polavieja, F. Borondo, and R.M. Benito, Phys. Rev. Lett. **73**, 1613 (1994); Int. J. Quantum Chem. **51**, 555 (1994).

[18] A.J. Lichtenberg and M.A. Lieberman, *Regular and Stochastic Motion* (Springer-Verlag, Berlin, 1983); J. Guckenheimer and P. Holmes, *Nonlinear Oscillations, Dynamical Systems and Bifurcations of Vector Fields* (Springer-Verlag, Berlin, 1983).

[19] A.M. Ozorio de Almeida, *Hamiltonian Systems: Chaos and Quantization* (Cambridge University Press, Cambridge, 1988).

[20] A.M. Ozorio de Almeida and J.H. Hannay, J. Phys. A **20**, 5873 (1987); C.P. Malta, M.A.M. de Aguiar, and A.M. Ozorio de Almeida, Phys. Rev. A **47**, 1625 (1993).

[21] J.M. Mao and J.B. Delos, Phys. Rev. A **45**, 1746 (1992); K.R. Meyer, J.B. Delos, and J.M. Mao (unpublished).

[22] M.W. Beims and G. Alber, Phys. Rev. A **48** 3123 (1993).

[23] A.M. Ozorio de Almeida and M.A.M. de Aguiar, Physica D **41**, 391 (1990).

[24] E.J. Heller, Phys. Rev. Lett. **53**, 1515 (1984); E.B. Bogomolny, Physica D **31**, 169 (1988).

[25] L.D. Landau and E.M. Lifshitz, *Mechanics* (Pergamon, New York, 1976).

[26] C.W. Gear, SIAM J. Num. Anal. **2**, 69 (1965).

[27] W.H. Press, S.A. Teukolsky, W.T. Vetterling, and B.P. Flannery, *Numerical Recipes* (Cambridge University Press, Cambridge, 1992).

[28] M.V. Berry and M. Tabor, Proc. R. Soc. London Ser. A **349**, 101 (1976).

[29] *Handbook of Mathematical Functions*, edited by M. Abramowitz and I.A. Stegun (Dover, New York, 1972).

[30] F.J. Harris, Proc. IEEE **66**, 51 (1978).

[31] J.M. Robbins, Phys. Rev. A **40**, 2128 (1989); W.T. Strunz, G. Alber, and J.S. Briggs, J. Phys. A **26**, 5157 (1993); P. Cvitanović and B. Eckhardt, Nonlinearity **6**, 277 (1993).

[32] K.M. Atkins and G.S. Ezra, Phys. Rev. A **50**, 93 (1994).

[33] H. Yoshida, Celestial Mechanics **32**, 73 (1984).

[34] M. Kuś, F. Haake, and D. Delande, Phys. Rev. Lett. **71**, 2167 (1993).

[35] M.V. Berry, Proc. R. Soc. London Ser. A **423**, 219 (1989); O. Agam and S. Fishman, J. Phys. A **26**, 2113 (1993); M. Feingold, Z. Phys. B **95**, 121 (1994).

[36] M.J. Davis, Chem. Phys. Lett. **192**, 479 (1992); Int. Rev. Phys. Chem. (to be published).

[37] M.J. Davis, C.C. Martens, R.G. Littlejohn, and J.S. Pehling, in *Advances in Molecular Vibrations and Collision Dynamics*, edited by J.M. Bowman and M.A. Ratner (JAI Press, Greenwich, 1991), Vol. 1B.

[38] K. Takahashi, Prog. Theor. Phys. Suppl. **98**, 109 (1989).